Review of Scientific Instruments

RESEARCH ARTICLE | SEPTEMBER 06 2023

Development of a cryogen-free sub-3 K low-temperature scanning probe microscope by remote liquefaction scheme

Ruisong Ma ; Hao Li ; Chenshuai Shi; Fan Wang ; Le Lei; Yuanzhi Huang; Yani Liu; Huan Shan; Li Liu; Shesong Huang ; Zhi-Chuan Niu; Qing Huan ; Hong-Jun Gao

Rev. Sci. Instrum. 94, 093701 (2023)
https://doi.org/10.1063/5.0165089

AIP Publishing

Review of Scientific Instruments ARTICLE pubs.aip.org/aip/rsi

Development of a cryogen-free sub-3 K low-temperature scanning probe microscope by remote liquefaction scheme

Cite as: Rev. Sci. Instrum. 94, 093701 (2023); doi: 10.1063/5.0165089
Submitted: 26 June 2023 • Accepted: 20 August 2023 •
Published Online: 6 September 2023

Ruisong Ma,[1] Hao Li,[2] Chenshuai Shi,[2] Fan Wang,[3] Le Lei,[1] Yuanzhi Huang,[1] Yani Liu,[1] Huan Shan,[1] Li Liu,[1] Shesong Huang,[3] Zhi-Chuan Niu,[4] Qing Huan,[1,5,6,a)] and Hong-Jun Gao[1,5,6,a)]

AFFILIATIONS

[1] Beijing National Laboratory for Condensed Matter Physics and Institute of Physics, Chinese Academy of Sciences, P.O. Box 603, Beijing 100190, China
[2] ACME (Beijing) Technology Co., Ltd., Bejing 101407, China
[3] Beijing Physike Technology Co., Ltd., Bejing 100085, China
[4] State Key Laboratory for Superlattices and Microstructures, Institute of Semiconductors, Chinese Academy of Sciences, Beijing 100083, China
[5] Songshan Lake Materials Laboratory, Dongguan, Guangdong 523808, China
[6] Key Laboratory for Vacuum Physics, University of Chinese Academy of Sciences, Beijing 100190, China

[a)] **Authors to whom correspondence should be addressed:** huanq@iphy.ac.cn and hjgao@iphy.ac.cn

ABSTRACT

We developed a new scheme for cryogen-free cooling down to sub-3 K temperature range and ultra-low vibration level. An ultra-high-vacuum cryogen-free scanning probe microscope (SPM) system was built based on the new scheme. Instead of mounting a below-decoupled cryocooler directly onto the system, the new design was realized by integrating a Gifford-McMahon cryocooler into a separate liquefying chamber, providing two-stage heat exchangers in a remote way. About 10 L of helium gas inside the gas handling system was cooled, liquefied in the liquefying chamber, and then transferred to a continuous-flow cryostat on the SPM chamber through an ~2 m flexible helium transfer line. The exhausted helium gas from the continuous-flow cryostat was then returned to the liquefying chamber for reliquefaction. A base temperature of ~2.84 K at the scanner sample stage and a temperature fluctuation of almost within ±0.1 mK at 4 K were achieved. The cooling curves, tunneling current noise, variable-temperature test, scanning tunneling microscopy and non-contact atomic force microscopy imaging, and first and second derivatives of I(V) spectra are characterized to verify that the performance of our cryogen-free SPM system is comparable to the bath cryostat-based low-temperature SPM system. This remote liquefaction close-cycle scheme shows conveniency to upgrade the existing bath cryostat-based SPM system, upgradeability of realizing even lower temperature down to sub-1 K range, and great compatibility of other physical environments, such as high magnetic field and optical accesses. We believe that the new scheme could also pave a way for other cryogenic applications requiring low temperature but sensitive to vibration.

I. INTRODUCTION

As essential tools in the field of condensed matter physics and surface science, the scanning tunneling microscopy (STM) and atomic force microscopy (AFM) enable researchers to image the atomic structure,[1,2] manipulate even a single atom,[3,4] and perform scanning tunneling spectroscopy (STS, dI/dV vs V)[5] and inelastic electron tunneling spectroscopy (IETS, d^2I/dV^2 vs V)[6] in atomic scale. On the basis of STM and AFM techniques, the scanning probe microscope (SPM) family was derived and developed.[7]

The low-temperature (LT) operations of SPMs significantly reduce the thermal drift, thermally induced noise, piezo-nonlinearities, and piezo-hysteresis.[8] That would give the SPM system a fundamental feasibility and stability in imaging, atom manipulation, and tunneling spectroscopy acquisition. More importantly, many physical properties, such as superconductivity,[9] Kondo

effect,[10] and Majorana fermions,[11] are restricted to the LT environment. Until now, most of the LT-SPMs adopted the bath[4,5,8,12,13] or continuous-flow cryostats[14,15] to achieve ~4 K by liquid helium-4 (^{4}He) for optimal performance in achieving low noise levels. In some other research fields, a helium-3 (^{3}He) refrigerator[16] or a ^{3}He/^{4}He dilution refrigerator[17,18] has been used to attain much lower temperature down to mK level.

Compared with the scheme of bath cryostat, the continuous-flow cryostat embodies many features, such as smaller volume, faster cooling rate, and feasibility in assembly, which has been proven to be a great success in the SPM field.[6,14,19] However, working at LT environment by the continuous-flow cryostat consumes much more liquid ^{4}He than the bath cryostat under the same cooling power. Therefore, most LT SPM systems adopt bath cryostats, in which the holding time can be a few days by just several L of liquid ^{4}He. However, these cryogenic instruments mentioned above heavily rely on liquid ^{4}He for cooling or precooling, which have been experiencing a price boom in recent decades. This situation now threatens the availability of the ^{4}He-based cryostats,[20] making the cryogen-free technology a promising way of coping with the ^{4}He resource shortage. In applications with a cryogen-free scheme, cryocoolers, such as Gifford-McMahon (GM) or pulse tube (PT) cryocoolers, are used to (pre-)cool the system to ~4 K or a lower temperature.[20]

These years, commercial GM[21,22] or PT[23] cryocoolers were also implemented in SPM systems due to the ^{4}He resource issue. However, the vibration oriented from the cryocoolers (μm level) severely disturbs the performance of the SPM system. Therefore, isolating the intrinsic vibration of the cryocooler from the tunneling junction should be paid much more attention. In these published cryogen-free SPM systems,[21–23] the cold head of the cryocoolers was top loaded above the SPM chamber and fixed on the strong supporting frame, which is tightly fixed on the ground. Bellows (rubber or stainless steel) act as vibration isolators, and the space inside the bellows is filled with a certain amount of ^{4}He gas for heat exchange. Rubber bellows have effective vibration isolation but a more significant permeability than stainless steel (SS) bellows, which reduces the reliability due to the freezing of the permeating gas. Meanwhile, when baking the SPM chamber, the cryocooler must be disassembled from the SPM chamber because the cryocooler cannot endure a higher temperature than 60 °C. In addition, with only ^{4}He gas being the heat exchanging medium, these cryostats merely achieved a base temperature of 9–15 K, which is not low enough for high-resolution tunneling spectroscopy and studying some temperature driven phenomena. UNISOKU Co., Ltd. developed a cryogen-free, PT cryocooler-based SPM, where both polytetrafluoroethylene (PTFE) and SS bellows are adopted in their design to achieve low permeability. They can obtain near-5 K temperature by liquefying the ^{4}He gas. To deal with the gas pressure fluctuation, they developed a programmatically controlled gas-handling system to automatically balance the gas pressure.[24] Recently, researchers from Fudan University have built a cryogen-free variable temperature SPM system based on a PT cryocooler in a similar configuration as above and the base temperature can be as low as 1.4 K with the help of a 1 K-pot above the scanner.[25] To maintain 0.5 L liquid ^{4}He, a large tank containing at least several hundred L of ^{4}He gas is adopted in their gas handling system. Therefore, the liquefaction of ^{4}He gas brought complexity and release risk to the cryogen-free systems.

In these existing cryogen-free SPM systems, the cryocooler was directly top-loaded near the SPM core component due to the assembly limitation of the cryocoolers. It seems easier to achieve better cooling performance; nevertheless, several shortcomings are also present as follows:

(1) The mechanical coupling between the cryocooler and the SPM is still strong, causing the noise level in a relatively high state.
(2) The physically assembled cryocooler close to the SPM module can only be installed vertically, which affects the expansibility of SPM functions, such as adding optical channels and magnetic fields, and baking operation for achieving ultra-high-vacuum (UHV). The magnetic fields will degrade the performance of the cryocooler, and high temperature will damage the cryocooler due to the presence of rare earth materials inside.
(3) To achieve a good vibration isolation effect, one or more independent fixed rigid frames are required to install the cryocooler and bellows. The independent frames take up a lot of space, affect the operation of the system, and are not convenient for the system to move.
(4) With only ^{4}He gas as the heat exchange medium, the base temperature can only reach ~10 K, which limits the further development of ^{3}He refrigerators to reach the sub-K temperature range following the present cryogen-free way for precooling. The way of liquefying ^{4}He gas requires a large amount of gas, and there may be a case of helium release, which greatly increases the operational complexity of the system.
(5) The present systems show high integration but poor upgradability since it is difficult to upgrade the bath cryostat-based SPM system by the reported cryogen-free schemes.

In this paper, we developed a UHV-LT-SPM system integrating a continuous-flow cryostat-based SPM subsystem and a novel GM cryocooler-based cryogen-free helium supply subsystem. The two subsystems are connected by a liquid ^{4}He transfer line and a ^{4}He gas return line of the gas handling system, which is filled with ~10 L helium gas in total. The GM cryocooler is assembled on a separate liquefying chamber and supported by specially SS bellows for vibration damping, where the ^{4}He gas is cooled by two-stage heat exchangers of the GM cryocooler cold head and further liquefied by throttling expansion. The liquid ^{4}He is transferred to the continuous-flow cryostat on the top of the SPM chamber through a long flexible liquid ^{4}He transfer line. Furthermore, an ~2.84 K base temperature at the scanner sample stage could be achieved by precisely adjusting the needle valve on the liquefying chamber. The pressure inside the circulation pipeline is automatically balanced by the edge welded SS bellow tank with the help of atmospheric pressure. The exhausted gas would be returned to the liquefying chamber through the return line. Consequently, an ultra-low vibration level can be obtained due to the remote cooling configuration. The performance of this cryogen-free SPM was demonstrated by cooling performance, noise spectrum, variable-temperature tests, SPM imaging, and STS and inelastic electron tunneling spectroscopy (IETS) measurements. These results show that our cryogen-free SPM system is comparable to conventional liquid ^{4}He-based SPM systems in terms of base temperature, stability, and data quality.

II. SYSTEM OVERVIEW

The developed cryogen-free SPM system mainly comprises two relatively independent subsystems: a continuous-flow cryostat-based SPM subsystem and a GM cryocooler-based cryogen-free helium supply subsystem. In this section, we will present the design of each part and the operation of the whole system.

A. SPM subsystem

The SPM subsystem comprises two chambers: an SPM chamber and a load-lock chamber, as shown in Fig. 1(a). A long transfer rod with six docking positions for sample holders and probe holders is mounted on the load-lock chamber and is used to transfer the holders between the two chambers, where there is another dock with six docking positions in the SPM chamber. A custom-designed annealing stage is integrated in the SPM chamber for *in situ* sample preparation, where the samples can be heated resistively or by the electron beam. An ion source (ACME IS 100-A) for Ar sputtering is assembled in the SPM chamber with a focus on the sample position of the annealing stage. A resistive heating evaporator (ACME RHE35A) is also assembled for NaCl deposition. The wobble stick in the SPM chamber can be used to transfer samples or probe holders. Both chambers are fixed on a bench frame supported by the pneumatic table to isolate the vibrations from the ground.

A continuous-flow cryostat (ARS LT3B) is mounted on the top flange (DN250CF) of the SPM chamber providing a cold head (<4 K) cooled by liquid ^{4}He and a cold shielding stage (tens of K) cooled by exhausting ^{4}He from the cold head. Correspondingly, two layers of thermal shields, namely inner shield and outer shield, are tightly fitted with the cold head and cold shielding stage of the continuous-flow cryostat, respectively. The top of the two layers of thermal shields are the gold coated copper plates (namely inner and outer shield Cu plates), and the rest of thermal shields are made of silver coated aluminum. The scanner is assembled inside the inner shield, as shown in the right part of Fig. 1(b). Our SPM scanner, an improved version based on Pan's design, is mainly composed of three parts: the unibody frame, the probe-approach module, and the sample stage, the detailed design of which has been reported in Ref. 12. In addition, two 75 Ω thin film resistors for variable-temperature measurements are installed on the scanner body. The Si diodes (DT670) are used to measure temperature at the continuous-flow cryostat cold head, the outer shield Cu plate, and the second cold stage of the GM cryocooler cold head. The fourth Si diode (calibrated Si410A) is directly attached to the back of the sample stage by silver conductive epoxy (EPO-TEK). The scanner is suspended by three springs with a calculated nature frequency of ~1.89 Hz. The vibrations in both lateral and vertical directions are further damped by eight SmCo magnets installed around the scanner on the bottom of the inner shield [Fig. 1(b)]. Several spiral copper braids link the inner shield Cu plate, scanner body, and sample stage to reduce the temperature gradient between them. Mechanically cut Pt–Ir probes are used for STM and STS measurements in this study. As for the non-contact AFM (NC-AFM) imaging, a 25 μm W wire is attached to the tuning fork (Nanosurf) and is electrochemically etched before use.

The signals transmitted from the scanner to the feedthroughs in the UHV chamber, such as high voltages for coarse motion and scanner, current for the heater, and IV signals of the temperature sensor, use twisted-pair manganin wires, which are thermally anchored both in the inner and in the outer shield Cu plates. As for the tunneling current (I_t), bias voltage (V_b), and NC-AFM signals, SS coaxial wires are used between feedthroughs and the inner shield Cu plate and then switched to Ag-plated alloy wires connecting to the terminals. To reduce crosstalk between sensitive signals, the wires for I_t, V_b, and NC-AFM signals are separated by at least 1 cm.

A 300 L/s turbo pump (Edwards nEXT300D) with a rotary pump as pre-stage can be used to pump the load-lock chamber, SPM chamber, or gas pipes between the leak valve and gas cylinders depending on the on–off status of the in-between valves. The base pressure of the load-lock chamber can be lower than 2×10^{-8} mbar. As for the SPM chamber, a base pressure of $<2 \times 10^{-10}$ mbar can be obtained and maintained by an ion getter pump (Agilent Varian VacIon Plus 300 StarCell Combination Pump) together with an attached titanium sublimation pump (TSP). Two leak valves are mounted independently on the ports in the SPM chamber for dosing Ar gas and CO gas, respectively. There is also a gate valve between the ion getter pump and the SPM chamber, which can be closed when dosing Ar gas for sputtering or venting the chamber for repair.

The control electronics are composed of a commercial current preamplifier (Femto DLPCA-200, 10^9 V/A), an LT charge amplifier (CREATEC) and a Nanonis SPM controller with a lock-in module (SPECS GmbH, Germany). The cooling curves of the temperature sensors in this paper can be recorded by the Lakeshore 336 and Java-based chart recorder software.

B. Cryogen-free helium supply subsystem

The cryogen-free helium supply subsystem is mainly composed of two closed ^{4}He circulation loops, as shown in Fig. 1(b). The first one is the ^{4}He circulation loop of the GM cryocooler (Sumitomo SRDK-415) and a helium compressor (Sumitomo F-50) connected by two helium transfer tubes. The GM cold head has two cold stages providing two corresponding heat exchangers (first and second) for the main ^{4}He circulation loop in our cryogen-free scheme, which connects the SPM subsystem and helium supply subsystem. The circulation pump built into the gas handling system (GHS) drives the main ^{4}He circulation loop. In this paper, the ^{4}He circulation loop is referred to this main circulation loop of the gas handling system. Inside the main circulation loop, ^{4}He gas exchanges heat with the first and second heat exchangers anchored on the GM cold head. After sufficient heat exchanging, the temperature of circulated ^{4}He can be reduced below 8 K and further liquefied through the throttling process with the needle valve. The cooled ^{4}He gas or liquid ^{4}He is introduced into the continuous-flow cryostat on the SPM chamber through a highly efficient liquid helium transfer line (length: ~2 m), and heat exchange is carried out within the continuous-flow cryostat. Then, the exhausted ^{4}He gas flows out of the continuous-flow cryostat through the return line and is again injected into the first and second heat exchangers within the liquefying chamber by the circulation pump (Edwards nXDS15i) to start a new cycle process. A faster cooling process can be realized by a circulation pump with a larger pumping speed.

As a result of the displacer motion in the GM cryocooler, vibration at the second cold stage of the GM cold head is on the order of 10 μm. However, since the resolution of SPM in the Z direction is on the order of 10 pm range, the total vibration noise transferred to the

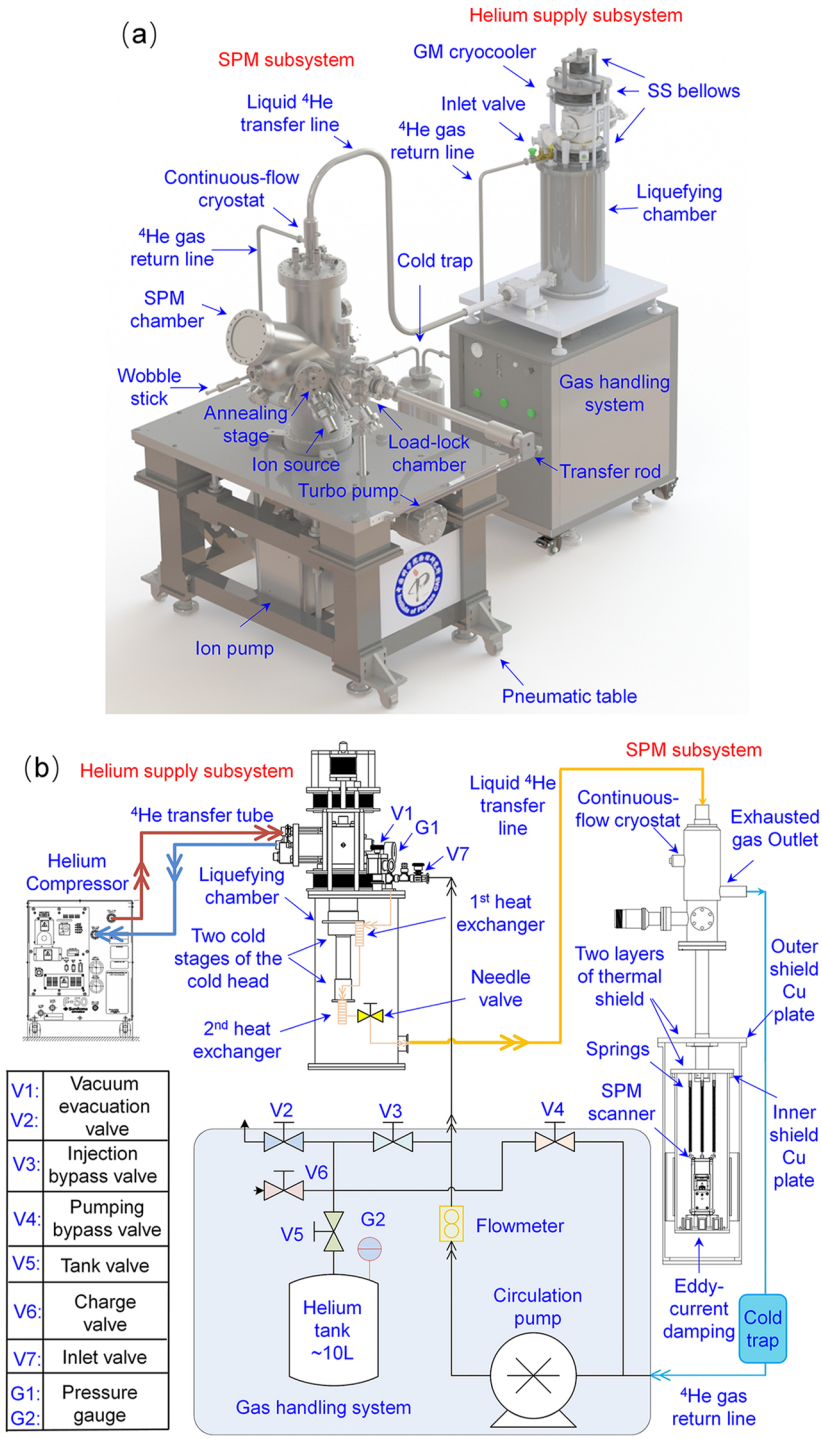

FIG. 1. 3D model and working schematic of the cryogen-free SPM system. (a) Isometric view of the entire cryogen-free SPM system. (b) Schematic showing the circulation of the cryogen-free SPM system. The figure is not drawn to scale. The inset sheet on the left shows some abbreviations of several valves and pressure gauges.

SPM tunneling junction should be limited to the pm range. Therefore, specially designed vibration isolation should be adopted for the GM cryocooler. In our scheme, the GM cryocooler is mounted on the liquefying chamber and levitated by three vibration isolation bellows. To achieve the optimal vibration isolation effect, the three bellows are designed in a pressure-balanced manner, which basically maintains the natural length of the bellows while supporting the GM cryocooler. As a result, when the cryocooler is in operation, the vibration transfer from the levitated cryocooler to the continuous-flow cryostat is effectively damped by the balanced SS bellows, which are nearly natural in terms of stress.

The GHS plays a crucial role in the main circulation of ^{4}He and cooling and maintenance of the cryogen-free system. Vacuum evacuation valve V1 is connected to the liquefying chamber of the GM cryocooler. An external pump set of a rotary pump and a turbo pump is used to vacuumize the liquefying chamber before and during the cooling-down process. The whole gas circulation pipeline can be vacuumized through vacuum evacuation valve V2 to remove the internal residual gas to prevent its freezing and resulting block of the gas circulation pipeline. As mentioned, the circulation pump, the power source of the GHS, drives the circulation of ^{4}He in the main circulation loop. The flowmeter and pressure gauge G1 monitor the helium flow and pressure of the circulation loop in real time, respectively. The ^{4}He gas is supplemented and recycled to the helium tank by injection bypass V3 and pumping bypass V4, respectively. V5 is the valve at the outlet of the helium tank, and pressure gauge G2 monitors the tank pressure. The helium tank is made of edge-welded SS bellows, which can automatically balance the pressure in the gas circulation pipeline (monitored by G1) close to 1 atm. When the ^{4}He gas is insufficient (excess), the gas can be injected into (ejected from) the tank through charge valve V6. V7 is the inlet of circulating gas at the GM cryocooler, which is connected to the outlet of the LT3B cryostat by the ^{4}He gas return line.

C. System operation

During the pumping down process of the cryocooler vacuum chamber and the gas circulation pipeline, V1–V4, V7, and the needle valve are fully open, and the circulation pump is kept on. After vacuum of the gas circulation pipeline reaches the order of 10^{-6} mbar, V2–V3 are closed and V5 is opened to fill the gas circulation pipeline with ^{4}He gas. The cold trap filled with liquid nitrogen is used to purify the circulating ^{4}He gas. When the pressure indicated by G2 on the helium tank is a little higher than 0 psi, V4 and V5 are closed. After that, the water chiller is turned on, and then, the helium compressor is started to cool down the GM cold head. During the cooling down process, the gas pressure within the gas circulation pipeline may be lowered due to partial liquefaction. Consequently, V3 and V5 are opened to automatically balance the pipeline pressure near 1 atm with the help of the edge welded SS helium tank.

Until the scanner sample stage reaches ~10 K, the needle valve is turned down to the status of about one third circle opening and the scanner is unclamped by adjusting the clamping mechanism to remove the direct contact with the two layers of the thermal shields. The scanner temperature could be finally lower than 3 K, and then, the cooling process is relatively slow. Finally, the scanner can achieve a minimal temperature drift by controlling the temperature with the help of two 75 Ω heaters and proportional–integral–derivative (PID) control using the temperature controller.

All operations regarding the SPM system, such as sample and probe transfer, clamping and unclamping, and shield opening and closing, can be realized with the wobble stick in the SPM chamber. The rotary pump and turbo pump in the SPM system are used to pump the SPM chamber when sputtering, annealing, and evaporating are carried out. During SPM measurements, only an ion getter pump is used to maintain vacuum of the SPM chamber.

When the circulation needs to be paused or stopped, by closing V7, opening V3 and V5, and fully tuning on the needle valve, the ^{4}He gas in the main gas circulation pipeline can be pumped back into the helium tank by the circulation pump. After the indication of G2 is stable, V5 can be closed. Then, the helium compressor and water chiller could be shut down if needed. The heaters on the scanner, continuous-flow cryostat, and GM cold head can all be used to accelerate the warming process. Until the temperature of the continuous-flow cryostat and cold head of the GM cryocooler increases to room temperature, the liquid ^{4}He transfer line and ^{4}He return line can be disassembled from the SPM system.

III. PERFORMANCE

To demonstrate the performance of our cryogen-free SPM system, we carried out cooling-down tests, power spectral density (PSD) measurements of the tunneling current vs frequency, SPM imaging, and tunneling spectroscopy measurements.

A. Cooling performance

One of the advantages of this design is that the system could work in two modes: the continuous-flow mode and the cryogen-free mode. We can use either liquid nitrogen or liquid ^{4}He for convenient and fast cooling from room temperature. For comparison, we first characterized the performance of the SPM system in the continuous mode with a liquid ^{4}He tank and a liquid ^{4}He transfer line. It takes about 6 and 12 h for the sample stage to reach <10 K and <5 K, respectively [Fig. 2(a)]. As in the case of cryogen-free mode, following the procedure described in Sec. II C, the scanner sample stage temperature can be below 10 K within less than 6 h. Then, by adjusting the needle valve and unclamping the scanner, the temperature can be rapidly reduced. It takes ~6.04 h for the scanner sample stage to reach temperature <4 K and ~8.60 h to be lower than 3 K from room temperature, as shown in the inset of Fig. 2(b). After additional 12 h, the final base temperature of ~2.84 K can be obtained as indicated in the inset of Fig. 2(b). In this case, the final temperature difference between the continuous-flow cryostat cold head and the sample stage is within 0.1 K due to the copper braids connecting them. We believe that the final base temperature could be further reduced by the optimization of thermal design to realize lower thermal loads, integration of cryocooler with a higher cooling power, and adoption of a wider circulation pipeline and a higher pumping-speed circulation pump. However, the noise level could be degraded in these cases, and further testing and optimization are needed.

The faster cooling and lower base temperature in the cryogen-free mode than in the continuous-flow mode can be attributed to the circulation pump and the throttle effect by the needle valve. Here, the needle valve function acts as a cryogenic variable flow

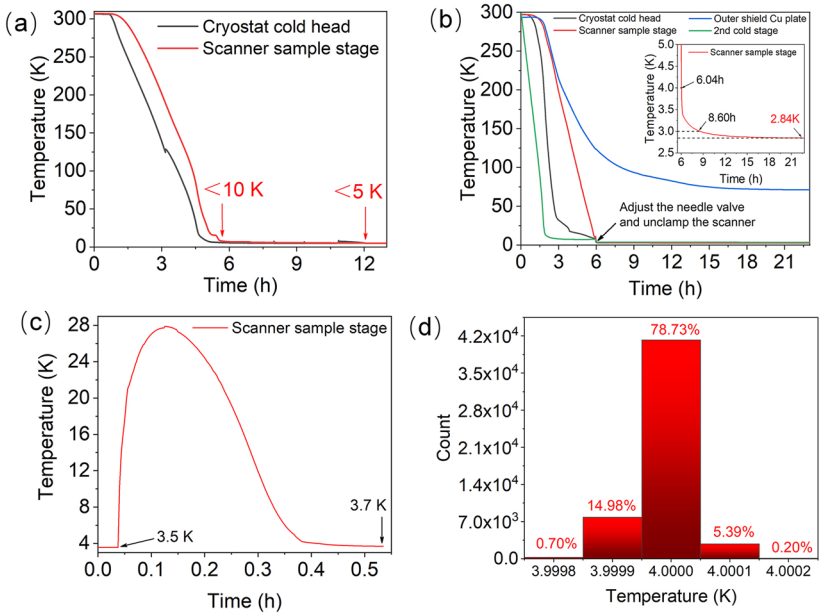

FIG. 2. Cooling performance and temperature stability of the cryogen-free SPM system. (a) Cooling down curves of continuous-flow cryostat cold head and scanner sample stage in the continuous-flow mode by a liquid ^{4}He tank. (b) Cooling down curves of cryostat cold head, scanner sample stage, second cold stage of the GM cryocooler, and outer shield Cu plate in the cryogen-free mode. The sample stage takes about 6 h to reach the temperature below 4 K and 8.6 h to be lower than 3 K. The base temperature of the scanner sample stage can be ~2.84 K. (c) Temperature variation after loading a room-temperature sample holder. It takes ~0.5 h to return to the original level. (d) Temperature histogram of the sample inside the SPM scanner controlled to stabilize at 4 K with the resistive heaters attached to the scanner body for three days. The histogram indicates that ~99.1% of the statistical temperature is within ±0.1 mK variation.

impedance, which can restrict helium flow and generate a proper pressure for efficient helium condensation. After fully precooling, the cold helium gas expands adiabatically by an external pump, and the helium cools thanks to the Joule–Thomson cooling effect. Therefore, the temperature becomes lower in the cryogen-free mode.

When exchanging sample or probe holders, the scanner should be clamped and the door on the two layers of the thermal shield should be opened, which results in a rapid temperature increase to ~28 K [Fig. 2(c)]. After closing the door, it takes half an hour for the scanner sample stage to return to a relatively low temperature level (below 3.7 K).

Since long-term temperature stability plays a vital role in SPM experiments, it is of importance to stabilize the base temperature. In our system, the 75 Ω heaters attached to the scanner body together with the temperature controller can be used to control the sample temperature by the PID algorithm. Figure 2(d) shows the statics of the temperature recorded over three days, indicating that a temperature fluctuation at 4 K is mainly within ±0.1 mK, while only 0.90% of data show ±0.2 mK fluctuation.

B. PSD measurement

The continuous-flow cryostat-based SPM showed low vibration noise and has been proved to be a success in SPM imaging and STS and IETS experiments at a single molecule level.[15,26,27] In comparison, we replaced the liquid ^{4}He tank in the continuous-flow mode with a cryogen-free helium supply subsystem instead, providing liquid ^{4}He for the continuous-flow cryostat in the SPM chamber. To demonstrate the vibration isolation effect in both continuous-flow and cryogen-free modes, we showed the PSD of the tunneling current signals, which directly reflects the stability of the probe-sample junction. Figure 3(a) shows the PSD curves of the tunneling current in the continuous mode as a function of frequency up to 1000 Hz with the probe retracted and tunneling with feedback on and off. In the withdrawn state, the basic noise is lower than 10 fA/Hz$^{1/2}$ in the full spectrum range. When the probe is engaged in the tunneling state with feedback on, the PSD level arises due to the tunneling current. When the feedback loop is turned off, the tunneling current is more sensitive to any changes, such as fluctuations of the probe–sample distance, and reaches a relatively higher state, especially in the low frequency range. However, even in the feedback off state, the noise is lower than 1 pA/Hz$^{1/2}$, indicating a considerably low noise level. The broad peak in the range from 3 to 10 Hz can be attributed to the pneumatic table, and the peak near 20 Hz may come from the spiral copper braids.

Then, we switch to the cryogen-free mode, the PSD results of which are shown in Fig. 3(b). In the case of probe retraction with GM on and off, the noise level is nearly the same and the noise baseline of both cases is between 1 and 10 fA/Hz$^{1/2}$, indicating a comparatively low level. As for the tunneling states with feedback on and off, the noise levels are slightly higher than the tunneling cases in the continuous-flow mode, which can be attributed to the participation of the circulation pump and GM cryocooler. Nevertheless, the

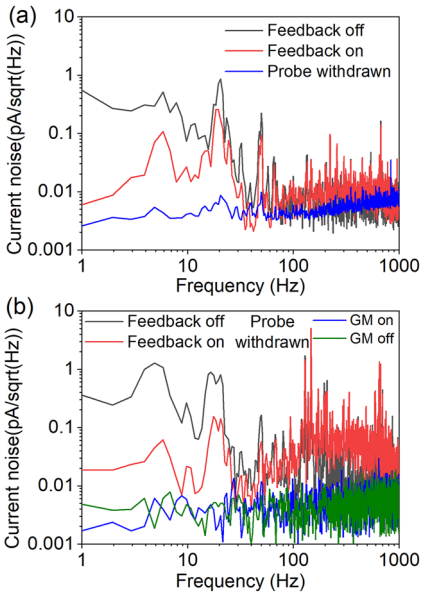

FIG. 3. Characterization of the noise spectrum by the power spectral density (PSD) of the tunneling current signals in (a) continuous-flow and (b) cryogen-free modes. These spectra are averaged with 300 continuously recorded curves. Tunneling conditions: tunneling current set point 100 pA, sample bias −100 mV, and sample Au(111).

absence of any peak in the range of 1–2 Hz (operating frequency of GM cryocooler) and the rareness of PSD intensity higher than 1 pA/Hz$^{1/2}$ indicate effective vibration isolation from the GM cryocooler. According to the results above, the vibration from the GM cryocooler and the lab environment has effectively been damped, laying a foundation for high-quality SPM imaging and tunneling spectroscopy measurement.

C. STM and STS performance

The performance of our cryogen-free SPM system in terms of STM and STS is acquired on Au(111) and Ag(110) substrates, prepared by repetitive Ar sputtering and annealing. Figures 4(a) and 4(e) show the large-area STM images of Au(111) and Ag(110) surfaces at 4 K, respectively, where herringbone reconstruction of Au(111) and terraces of Ag(110) can be clearly seen. The atomic-resolved STM images of Au(111) and Ag(110) surfaces are demonstrated in Figs. 4(b) and 4(f), while atom corrugations indicated by the line profiles along the red lines are shown in Figs. 4(c) and 4(g), respectively. Accordingly, the height noise along the Z direction is lower than 1 pm. Figure 4(d) shows the STS result of the face-centered cubic (FCC) and hexagonal close-packed (HCP) positions on the Au(111) surface, and Fig. 4(h) displays the STS spectra on the flat area of the Ag(110) surface, consistent with the reported results.[22,28]

As a key indicator of the SPM system, the minimum tunneling current for STM imaging also reflects the noise level of both the instrument and the equipped electronics. Figures 5(a)–5(f) show the STM images of Au(111) surface obtained with V_b = −1 V and the tunneling current set at 5.0, 3.0, 2.0, 1.5, 1.0, and 0.8 pA, respectively, by an external preamplifier at 10^9 V/A gain. As can be seen in Fig. 5, the image resolution decays as the tunneling current is reduced gradually and a stable tunneling junction cannot be formed

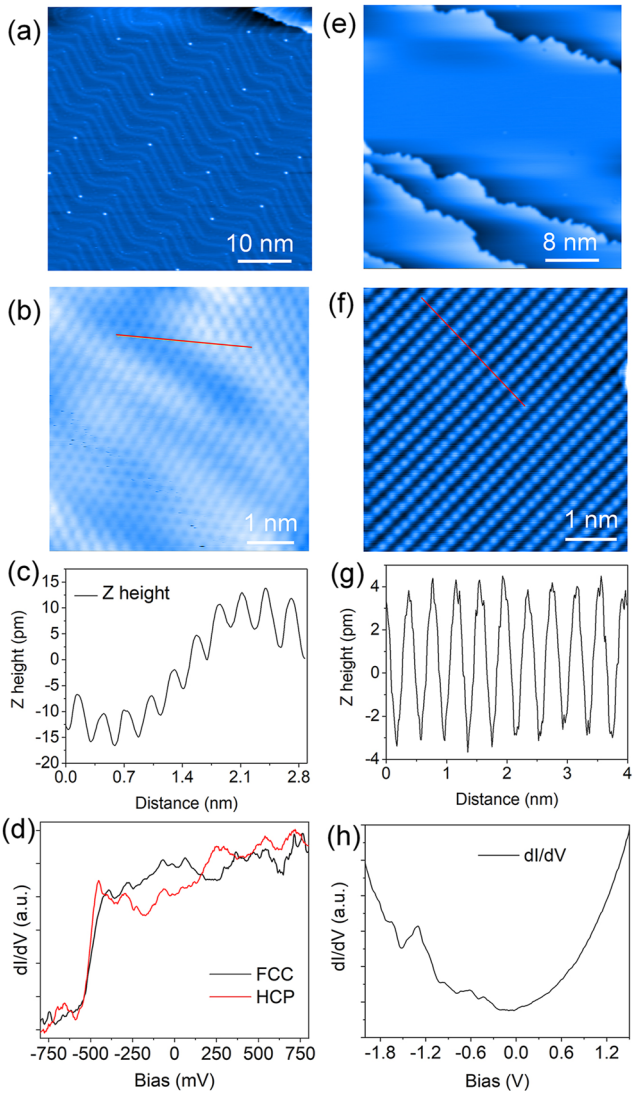

FIG. 4. Characterization of the STM performance by the imaging and tunneling spectroscopy on Au(111) and Ag(110) substrates. (a) Herringbone reconstruction of the Au(111) surface. I_t = 100 pA and V_b = −1 V. (b) Atomic resolution of the Au(111) surface. I_t = 112.3 pA and V_b = 1 V. (c) Line profile of the Au atoms along the red line shown in (b). (d) Single-pass dI/dV spectra at the FCC and HCP sites of the Au(111) surface. The STM feedback is turned off during the dI/dV spectra process with a gap set at 500 pA/−180 mV. The dwell time per point is 55 ms, and the bias modulation is set as 1 mVrms@425.36 Hz. (e) Large-area STM image of the Ag(110) surface. I_t = −641.7 pA and V_b = −2 V. (f) Atomic-resolved STM image of the Ag(110) surface. I_t = 5 nA and V_b = −50 mV. (g) Line profile of the Ag atoms along the red line shown in (f). (h) The dI/dV spectra at the Ag(110) surface. The gap is set at 577.3 pA/−2 V before turning off the feedback. The dwell time per point is 170 ms, and the bias modulation is set as 4 mVrms@407.806 Hz.

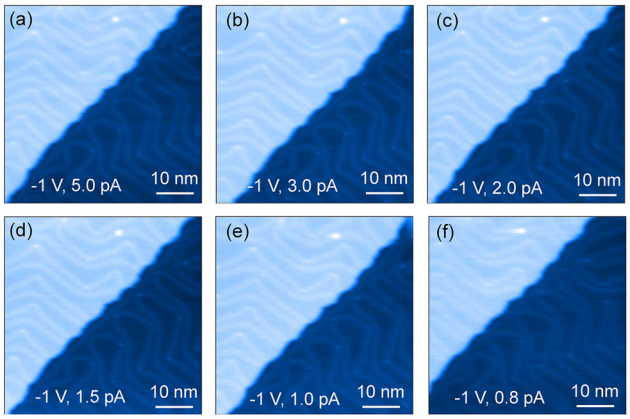

FIG. 5. Minimum tunneling current measurement for STM imaging. STM images of Au(111) are obtained with −1 V bias and the tunneling current set at 5.0 pA (a), 3.0 pA (b), 2.0 pA (c), 1.5 pA (d), 1.0 pA (e), and 0.8 pA (f).

at a lower current set point than 0.8 pA. Consequently, we can conclude that the minimum scanning tunneling current is lower than 1 pA, comparable to the SPM system with a bath cryostat.

To demonstrate the thermal stability of the SPM, we carried out a thermal drift test at 4 K. The average thermal drift of the scanner in lateral and vertical directions is ~10 and ~5 pm/h, respectively, which is tested by a continuous scanning of 16 h at a fixed area on the Au(111) sample with I_t = 100 pA and V_b = −100 mV.

As is known, many material systems exhibit different exotic physical properties in different temperature ranges. Therefore, it is of vital importance to carry out variable temperature experiments. Figure 6 shows the results of variable-temperature tests from 3.5 to 300 K. It takes about an hour to stabilize the scanner temperature within ±1 mK at the evaluated temperatures mentioned above, demonstrated by the temperature variations at 20 K as an example (upper right inset in Fig. 6). The inset STM images in Fig. 6

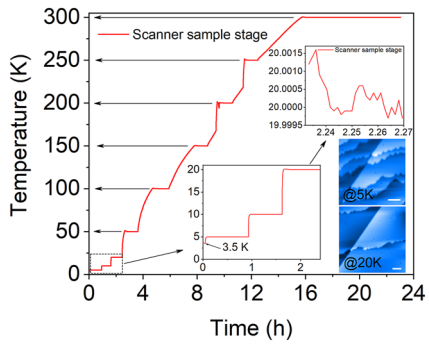

FIG. 6. Variable-temperature tests from 3.5 to 300 K. The arrows point to the stabilized temperature at the corresponding platform. The stability at each temperature set point can be lower than ±1 mK after a 1 h PID adjustment. The inset figures on the middle bottom show the zoom-in temperature curve from 3.5 to 20 K. The temperature variations at 20 K are gradually reduced to the ±1 mK range, as shown in the inset on the top right. Two STM images obtained at 5 and 20 K, respectively, are inset on the right. The scale bar in the inset denotes 5 nm. Tunneling conditions: I_t = 100 pA and V_b = −1 V.

present the terrace structures of the Ag(110) surface at 5 and 20 K for demonstration. The corresponding calibration coefficients of the scanner at different temperatures must be set before the imaging process.

D. IETS and microscopy

The STS mentioned above, i.e., dI/dV, assumes that electrons tunnel without losing the energy in an elastic way. However, in addition to the elastic tunneling process, the inelastic tunneling process also occurs when V_b exceeds the energy required to excite some states, such as molecular vibration modes on the surface, contributing a small portion of additional inelastic tunnel electrons.[26,29] The IETS signal, which is proportional to the second derivative of I(V), i.e., d^2I/dV^2, is relatively weak and is usually measured by recoding the second harmonic signals with respect to the modulation bias voltage at a specified frequency from the built-in lock-in amplifier. As a result, the STM-based IETS measurements at the atomic level are experimentally involved, which require an extremely high signal-to-noise ratio and high stability at low temperatures.[30]

Thanks to the excellent performance in terms of tunneling current noise and thermal stability, the developed cryogen-free SPM system enables us to carry out IETS and microscopy measurements on single molecules. The CO molecules were dosed to adsorb on the Cu(111) and Ag(110) surfaces, sputtered, and annealed several times. Figure 7 shows the IETS results on Cu(111), consisting of the frustrated translational (FT) and frustrated rotational (FR) modes located at ~7 and ~35 mV, respectively. The inset of Fig. 7 shows that the CO molecules appear as depressed "dark" spots in the STM image.

Figure 8(a) shows the STM image of three CO molecules on the Ag(110) substrate at 4 K. By positioning the probe to CO molecules on the left-bottom corner and setting the tunneling current to ~1 nA, the probe will pick up the molecule. Henceforth, the imaging resolution becomes much higher than before, and the CO molecule appears as a donut located on the Ag atom chain along [1$\bar{1}$0], as shown in Fig. 8(b). Furthermore, in our case, the CO-adsorbed probe is stable even at 6 nA tunneling current set point. Therefore, we performed IETS measurements with the CO adsorbed probe at the bare Ag area. The d^2I/dV^2 spectra shown in Fig. 8(c) are averaged for

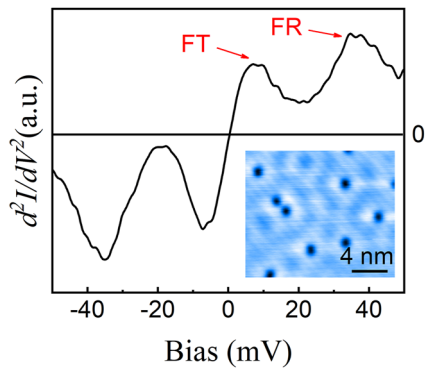

FIG. 7. IETS measurement of CO molecules on the Cu(111) substrate. The FT and FR modes of the CO are resolved. The tunnel gap is set at 5 nA/50 mV with a bias voltage modulation set as 5 mV/525 Hz.

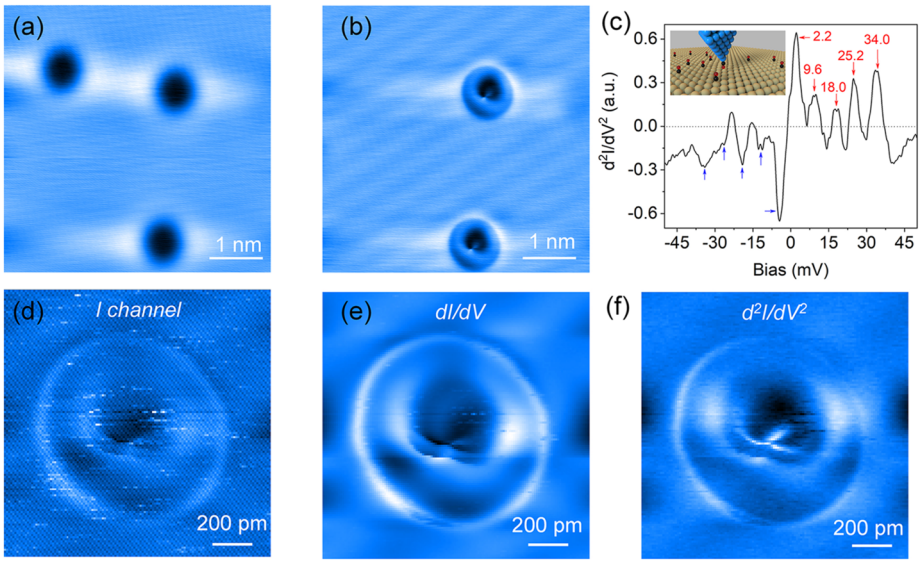

FIG. 8. IETS mapping of CO molecules on the Ag(110) substrate with a CO-adsorbed Pt–Ir probe. (a) STM images of CO molecules adsorbed on the Ag(110) surface shown as a black dip. I_t = 235.3 pA and V_b = 100 mV. (b) High-resolution STM image of CO molecules with a CO adsorbed Pt–Ir probe. The adsorbed CO molecule is initially located at the upper-left corner in (a). I_t = 235.3 pA and V_b = 50 mV. (c) IETS spectra obtained with a CO-adsorbed probe on the bare Ag surface. Several peaks emerge, which can be attributed to the FT (2.2 and 9.6 meV) and FR (18.0 and 25.2 meV) modes and overtone of the FR mode (34.0 meV). The feedback is turned off during data acquisition with a dwell time of 220 ms per point. The tunnel gap is set at 5 nA/50 mV with a bias modulation set to 5 mVrms@387.39 Hz. (d) Tunneling current, (e) dI/dV, and (f) d^2I/dV^2 mapping of a single CO molecule on the Ag(110) substrate with a CO-adsorbed Pt–Ir probe. The feedback is kept on during data acquisition with 170 ms per point (128 × 128 pixels). The tunnel gap is set at 110 pA/9.6 mV with a bias modulation set to 5 mVrms@387.39 Hz.

10 passes, where several peaks emerge due to the different vibration modes of CO molecules. The feedback was turned off during the spectra measurement with a dwell time of 220 ms per point. The tunnel gap was set at 5 nA/50 mV with the bias modulation of 5 mVrms@387.39 Hz. The peaks at 2.2 and 9.6 meV can be attributed to the FT mode, while 18.0 and 25.2 meV peaks are relevant to the FR mode.[31,32] The overtone of the FR mode can also be seen at 34.0 meV. The peak intensity asymmetry can result from the difference in strength between the molecule–probe coupling and the molecule–substrate coupling.[33]

Moreover, we have obtained the microscopy of a single CO molecule by the CO adsorbed probe in the aspect of tunneling current, dI/dV, and d^2I/dV^2, as demonstrated in Figs. 8(d)–8(f), respectively. The feedback loop is enabled during data acquisition with 170 ms per point (128 × 128 pixels in total). The tunnel gap was set to 110 pA/9.6 mV with a bias modulation of 5 mVrms@387.39 Hz. The CO molecule appears as s bright ring with fine structures in the middle. With the IETS and microscopy shown above, we can conclude that the signal-to-noise ratio and stability of our cryogen-free SPM are as high as the bath cryostat-based SPM.

E. NC-AFM performance

After replacing the STM probe holder with the qPlus sensor holder, our cryogen-free SPM system can perform both STM and NC-AFM. The frequency sweep of a qPlus sensor [Fig. 9(a)] demonstrates a center frequency of ~29 kHz and a typical Q factor of >42 000 at 4 K. The background noise of the oscillation amplitude

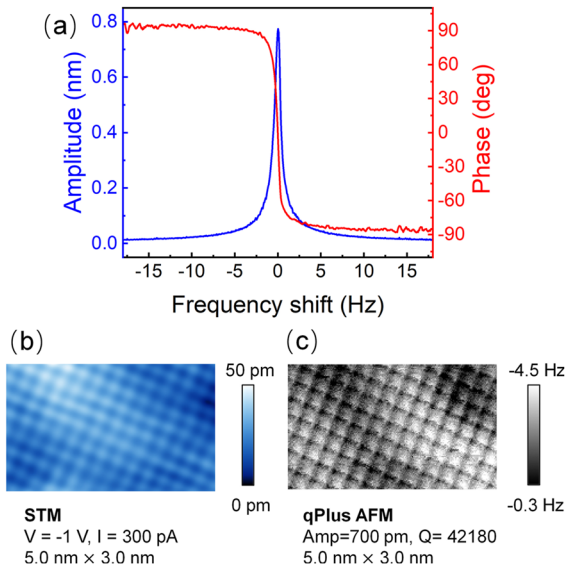

FIG. 9. Performance characterization of the NC-AFM mode in the cryogen-free SPM system. (a) Sweeping frequency curve of a qPlus sensor mounted with a W probe (wire diameter d = 25 μm) at 3.5 K. The center frequency is 28 933.4 Hz, and Q is 421 80. (b) Constant-current STM image of bilayer NaCl(100) on Au(111) at 3.5 K. (c) Constant-height (Δf) AFM image of the same area as in (b). Tunneling conditions: I_t = 300 pA and V_b = −1 V. The AFM oscillation amplitude is 700 pm. Size: 5.0 × 3.0 nm^2.

without external excitation is about 3 pm for a calibrated qPlus sensor in our cryogen-free SPM system at 4 K. To demonstrate the performance of NC-AFM based on the qPlus sensor,[34] we deposited NaCl onto the Au(111) surface at room temperature to produce crystallized bilayer NaCl(100) islands.[35] Figure 9(b) shows the STM image of bilayer NaCl(100) islands by the qPlus sensor, in which the atomic structure can be clearly resolved. Next, we performed NC-AFM measurements on the same area in the constant height mode. The atomic-resolution AFM frequency-shift (Δf) image shown in Fig. 9(c) also indicates the excellent stability of our cryogen-free SPM system.

IV. Further Application

As we know, SPM systems need to be operated in LT environments to achieve low noise levels and high energy resolution. In the mainstream SPM system working on 4 K, the cryogenic environment is mainly obtained by filling the bath cryostat with liquid nitrogen and liquid ^{4}He as refrigerants. However, such a refrigerating mode cannot maintain a long-time LT because the refrigerant must be refilled after exhaustion. The typical holding time with 4 L ^{4}He is about 3–4 days. The system must be interrupted during the refilling process, and thus, long-term data acquisition, such as high-resolution IETS mapping, cannot be realized.

Figure 10(a) shows the 3D model of such a typical bath cryostat-based SPM system with a load-lock, a molecular beam epitaxial (MBE), and a SPM chamber, the design and performance of which have been reported in Ref. 12. We have successfully upgraded this system to cryogen-free SPM by directly replacing the bath cryostat with the continuous-flow cryostat and the cryogen-free helium supply system, as shown in Fig. 10(b). The original scanner, thermal shields, and other components ever mounted with the bath cryostat can be reused if applicable during the upgrading process. Both the prototype shown above and the upgraded cryogen-free SPM system have been operated for at least two months while data acquiring and testing. As a result, this upgrading scheme can also be applied to other LT SPM systems faced with a long-term testing demand.

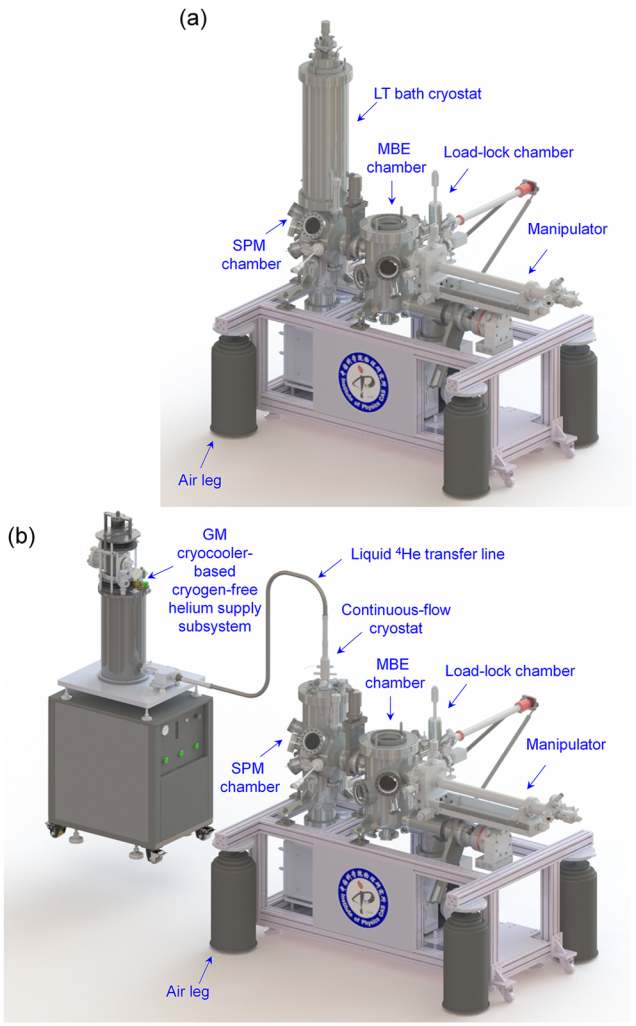

FIG. 10. 3D model showing the replacement of LT bath cryostat by a cryogen-free He supply system in an SPM system. (a) Schematic drawing of an LT SPM system with a load-lock, an MBE, and an SPM chamber. The LT environment is provided by LT liquid nitrogen and liquid ^{4}He bath cryostats. (b) Replacement of LT bath cryostat in (a) by a GM cryocooler-based helium supply subsystem.

V. CONCLUSION

To summarize, we have developed a new cryogen-free LT SPM system by a remote liquefaction scheme, which reaches ~2.84 K base temperature of sample stage and shows excellent performance in SPM imaging, STS, and IETS and is comparable to the current mainstream bath cryostat based SPM. To reduce the influence of vibration from the cryocooler, a separate liquefying chamber is mounted on the cryocooler for heat exchange with ^{4}He gas. Liquefied ^{4}He is transferred to the SPM continuous-flow cryostat by a soft helium transfer line. Moreover, a specially designed vibration isolation module made of three edge welded SS bellows supports the GM cryocooler and can dampen the vibrations since they are self-balanced and always in a near natural state. In addition to achieving significantly lower temperatures and ultra-low vibration levels, this closed-loop remote liquefaction scheme offers the advantage of conveniently upgrading existing wet SPM systems based on bath cryostats. In addition, it offers increased potential for upgradeability of realizing sub-1 K range with ^{3}He precooled by this cryogen-free scheme, as well as great compatibility with additional physical environments, such as high magnetic fields and optical access. Our remote liquefaction cryogen-free scheme can also be integrated with other applications requiring an LT environment while sensitive to vibration.

ACKNOWLEDGMENTS

The authors are grateful to Professor Hui Chen (IOP, CAS) for helpful discussions. The authors would also like to thank Miss Nahia for her technical assistance with the schematic drawing. This work was supported by the National Science Fund for Distinguished Young Scholars (Grant No. T2125014), the Special Fund for Research on National Major Research Instruments of NSFC (Grant No. 11927808), the CAS Key Technology Research and Development Team Project (Grant No. GJJSTD20200005), the National

Natural Science Foundation of China (Grant No. 12004417), and the Huairou Science Center of Beijing Municipal Science and Technology Project (Grant No. Z191100002019021).

AUTHOR DECLARATIONS

Conflict of Interest

The authors have no conflicts to disclose.

Author Contributions

Ruisong Ma: Data curation (equal); Formal analysis (equal); Investigation (equal); Validation (equal); Writing – original draft (equal); Writing – review & editing (equal). **Hao Li**: Data curation (supporting); Methodology (equal); Validation (equal). **Chenshuai Shi**: Data curation (supporting); Methodology (equal); Validation (equal). **Fan Wang**: Investigation (equal); Methodology (equal); Validation (equal). **Le Lei**: Data curation (supporting); Formal analysis (supporting); Writing – review & editing (supporting). **Yuanzhi Huang**: Data curation (supporting); Formal analysis (supporting); Writing – review & editing (supporting). **Yani Liu**: Data curation (supporting); Formal analysis (supporting); Investigation (supporting); Writing – review & editing (supporting). **Huan Shan**: Data curation (supporting); Formal analysis (supporting); Writing – review & editing (supporting). **Li Liu**: Software (lead). **Shesong Huang**: Conceptualization (equal); Investigation (equal); Methodology (equal). **Zhi-Chuan Niu**: Methodology (equal); Resources (supporting). **Qing Huan**: Conceptualization (equal); Resources (equal); Supervision (equal); Writing – review & editing (equal). **Hong-Jun Gao**: Project administration (lead); Resources (equal); Supervision (equal); Writing – review & editing (equal).

DATA AVAILABILITY

The data that support the findings of this study are available from the corresponding authors upon reasonable request.

REFERENCES

[1]G. Binnig, H. Rohrer, C. Gerber, and E. Weibel, Appl. Phys. Lett. **40**(2), 178–180 (1982).
[2]F. J. Giessibl, Science **267**(5194), 68–71 (1995).
[3]D. M. Eigler and E. K. Schweizer, Nature **344**(6266), 524–526 (1990).
[4]G. Meyer, Rev. Sci. Instrum. **67**(8), 2960–2965 (1996).
[5]S. A. Elrod, A. L. de Lozanne, and C. F. Quate, Appl. Phys. Lett. **45**(11), 1240–1242 (1984).
[6]B. Stipe, M. Rezaei, and W. Ho, Science **280**(5370), 1732–1735 (1998).
[7]K. Bian, C. Gerber, A. J. Heinrich, D. J. Müller, S. Scheuring, and Y. Jiang, Nat. Rev. Methods Primers **1**(1), 36 (2021).
[8]M. Z. Baykara, M. Morgenstern, A. Schwarz, and U. D. Schwarz, in *Springer Handbook of Nanotechnology*, edited by B. Bhushan (Springer Berlin Heidelberg, 2017).
[9]S. Qin, J. Kim, Q. Niu, and C.-K. Shih, Science **324**(5932), 1314–1317 (2009).
[10]V. Vaňo, M. Amini, S. C. Ganguli, G. Chen, J. L. Lado, S. Kezilebieke, and P. Liljeroth, Nature **599**(7886), 582–586 (2021).
[11]D. Wang, L. Kong, P. Fan, H. Chen, S. Zhu, W. Liu, L. Cao, Y. Sun, S. Du, J. Schneeloch, R. Zhong, G. Gu, L. Fu, H. Ding, and H.-J. Gao, Science **362**(6412), 333–335 (2018).
[12]Z.-B. Wu, Z.-Y. Gao, X.-Y. Chen, Y.-Q. Xing, H. Yang, G. Li, R. Ma, A. Wang, J. Yan, C. Shen, S. Du, Q. Huan, and H.-J. Gao, Rev. Sci. Instrum. **89**(11), 113705 (2018).
[13]G. He, Z. Wei, Z. Feng, X. Yu, B. Zhu, L. Liu, K. Jin, J. Yuan, and Q. Huan, Rev. Sci. Instrum. **91**(1), 013904 (2020).
[14]S. Behler, M. K. Rose, J. C. Dunphy, D. F. Ogletree, M. Salmeron, and C. Chapelier, Rev. Sci. Instrum. **68**(6), 2479–2485 (1997).
[15]B. C. Stipe, M. A. Rezaei, and W. Ho, Rev. Sci. Instrum. **70**(1), 137–143 (1999).
[16]S. H. Pan, E. W. Hudson, and J. C. Davis, Rev. Sci. Instrum. **70**(2), 1459–1463 (1999).
[17]Y. J. Song, A. F. Otte, V. Shvarts, Z. Zhao, Y. Kuk, S. R. Blankenship, A. Band, F. M. Hess, and J. A. Stroscio, Rev. Sci. Instrum. **81**(12), 121101 (2010).
[18]D. Wong, S. Jeon, K. P. Nuckolls, M. Oh, S. C. J. Kingsley, and A. Yazdani, Rev. Sci. Instrum. **91**(2), 023703 (2020).
[19]H. Lee and W. Ho, Science **286**(5445), 1719–1722 (1999).
[20]Z. Zhao and C. Wang, *Cryogenic Engineering and Technologies: Principles and Applications of Cryogen-Free Systems* (CRC Press, 2019).
[21]J. D. Hackley, D. A. Kislitsyn, D. K. Beaman, S. Ulrich, and G. V. Nazin, Rev. Sci. Instrum. **85**(10), 103704 (2014).
[22]S. Zhang, D. Huang, and S. Wu, Rev. Sci. Instrum. **87**(6), 063701 (2016).
[23]S. Chaudhary, J. J. Panda, S. Mundlia, S. Mathimalar, A. Ahmedof, and K. V. Raman, Rev. Sci. Instrum. **92**(2), 023906 (2021).
[24]J. Kasai, T. Koyama, M. Yokota, and K. Iwaya, Rev. Sci. Instrum. **93**(4), 043711 (2022).
[25]H. Huang, M. Shuai, Y. Yang, R. Song, Y. Liao, L. Yin, and J. Shen, Rev. Sci. Instrum. **93**(7), 073703 (2022).
[26]W. Ho, J. Chem. Phys. **117**(24), 11033–11061 (2002).
[27]C. Xu, C.-l. Chiang, Z. Han, and W. Ho, Phys. Rev. Lett. **116**(16), 166101 (2016).
[28]T. Andreev, I. Barke, and H. Hövel, Phys. Rev. B **70**(20), 205426 (2004).
[29]M. A. Reed, Mater. Today **11**(11), 46–50 (2008).
[30]Z. Novotny, Z. Zhang, and Z. Dohnálek, in *Encyclopedia of Interfacial Chemistry*, edited by K. Wandelt (Elsevier, Oxford, 2018).
[31]J. Oh, H. Lim, R. Arafune, J. Jung, M. Kawai, and Y. Kim, Phys. Rev. Lett. **116**(5), 056101 (2016).
[32]D. Kuhness, J. Pal, H. J. Yang, N. Mammen, K. Honkala, H. Häkkinen, W.-D. Schneider, M. Heyde, and H.-J. Freund, Top. Catal. **63**(15), 1578–1584 (2020).
[33]Z. Han, G. Czap, C. Xu, C.-l. Chiang, D. Yuan, R. Wu, and W. Ho, Phys. Rev. Lett. **118**(3), 036801 (2017).
[34]F. J. Giessibl, Rev. Mod. Phys. **75**(3), 949–983 (2003).
[35]J. Guo, X. Meng, J. Chen, J. Peng, J. Sheng, X.-Z. Li, L. Xu, J.-R. Shi, E. Wang, and Y. Jiang, Nat. Mater. **13**(2), 184–189 (2014).